We are IntechOpen, the world's leading publisher of Open Access books Built by scientists, for scientists

6,900
Open access books available

186,000
International authors and editors

200M
Downloads

Our authors are among the

154
Countries delivered to

TOP 1%
most cited scientists

12.2%
Contributors from top 500 universities

CLARIVATE ANALYTICS
BOOK CITATION INDEX
INDEXED

WEB OF SCIENCE™

Selection of our books indexed in the Book Citation Index
in Web of Science™ Core Collection (BKCI)

Interested in publishing with us?
Contact book.department@intechopen.com

Numbers displayed above are based on latest data collected.
For more information visit www.intechopen.com

Study of CO$_2$ Decomposition in Microwave Discharges by Optical Diagnostic Methods

Tiago Silva, Nikolay Britun, Thomas Godfroid and
Rony Snyders

Additional information is available at the end of the chapter

Abstract

The increasing of the carbon dioxide (CO$_2$) release into the atmosphere is undeniably one of the biggest concerns for the twenty-first century. Among the different strategies proposed for reduction of CO$_2$ emission (carbon capture and sequestration (CCS), renewable energies, etc.), low-temperature plasma technology offers an alternative and rather efficient way to convert CO$_2$ into the valuables chemicals (e.g. syngas) which can be stored and used afterwards. Several CO$_2$ decomposition plasma-related approaches have been proposed in the literature, all having a main task: increasing the energy efficiency associated to the decomposition process, while keeping the conversion rate at reasonably high level. This task is especially challenging since many kinetic mechanisms of CO$_2$ decomposition in low-temperature discharges are not yet well-known, such as the vibrational excitation which plays a key role in achieving high decomposition rates. In this chapter our recent research efforts associated with the experimental study of the CO$_2$ decomposition in microwave surfaguide low-temperature discharges are presented. The research was focused on the systematic investigation of the basic plasma parameters. The discharge area of the reactor was characterized by optical emission spectroscopy using the light emitted from spontaneous relaxation of excited species in plasma. The critical parameters such as gas temperature and dissociation rate were evaluated. In addition to this, the post-discharge area was characterized by two-photon absorption laser-induced fluorescence and gas chromatography techniques in order to investigate the exhaust gas composition. All together, the results overviewed in this chapter provide interesting insights into different kinetic mechanisms of CO$_2$-containing discharges, which play an important role in the CO$_2$ decomposition process.

Keywords: CO$_2$ decomposition, microwave discharge, optical emission spectroscopy, two-photon absorption laser-induced fluorescence, gas chromatography

1. Introduction

The combustion of coal, oil, and natural gas supplies approximately 87% of the primary energy used worldwide [1]. These anthropogenic activities are the main sources of CO_2 emission, which is well known for its contribution to the greenhouse effect and planetary heating. Currently, we are burdening the atmosphere of our world with an additional 40 billion tons of CO_2 every year [2]. Furthermore, the rate of these emissions is dramatically increasing as the world population grows and new economies are developed. As recently reported by the National Oceanic and Atmospheric Administration (NOAA), the level of CO_2 accumulated in the atmosphere has reached a symbolic milestone of 400 parts per million (ppm) [3]. This is the highest level of atmospheric CO_2 in human history. In fact, the planet has not experienced these levels of CO_2 since the *Pliocene* period (more than three million years ago). At this point, we are facing a global warming trend which is undoubtedly one of the biggest concerns for the twenty-first century. The scientific evidence concerning numerous drastic effects on the actual earth's physical and biological systems is overwhelming. Serious consequences include the melting of glaciers, loss of biodiversity, change in the agricultural productivity, etc. Unless we find efficient solutions to reduce our reliance on fossil fuels, the planet will continue to warm up in the coming decades and greater will be the impact of climate change.

1.1. The recycling of CO_2

One of the most promising solutions to stabilize the amount of greenhouse pollution in the atmosphere is the so-called *carbon capture and utilization* (CCU) [4]. Such an approach attempts to use CO_2, either directly or after chemical conversion, as part of a reaction chain to produce value-added products. The supply of CO_2 at local level would be guaranteed in the long term by various sources, from small smoke stacks to large coal-fired plants. In this regard, CCU is a very attractive strategy from an economic point of view, considering that in the near future, large amounts of CO_2 will become available as feedstock of nearly zero or even negative cost [5]. In addition, given the possibility of having cheap renewable energy (e.g., wind power during the night period [5]), there is a huge potential in combining the CCU with CO_2-free electricity. This last point is considered to be a key aspect toward a more general goal of resource since it combines the efficient reuse of a waste followed by the reduction of fossil fuel combustion [6]. An overview on different ways to convert CO_2 with the specific reference of introducing renewable energy in the chemical production chain is given in [6, 7]. Among the different CCU routes, the CO_2 hydrogenation is widely discussed nowadays. This strategy is based on the water-gas shift reaction (WGSR):

$$CO + H_2O \Leftrightarrow CO_2 + H_2 \tag{1}$$

to produce syngas (mixture of CO/H_2) which can be further utilized as a building block of methanol, dimethyl ether, liquid hydrocarbons, and other useful compounds via the Fischer-Tropsch process [7]. The intrinsically high energy density of these fuels and their good transportability make them highly desirable. Figure 1 shows an idealized energy cycle that combines renewable energies with CCU valorization through the WGSR. The CO_2 is recovered from an emission source and transformed into liquid fuels, provided that a sustainable production of CO via renewable electricity is obtained. This is an extremely

practical case in which the net production of CO$_2$ would be zero, while the renewable energy could be stored in CO$_2$-neutral fuels to be integrated in the existing transport infrastructure.
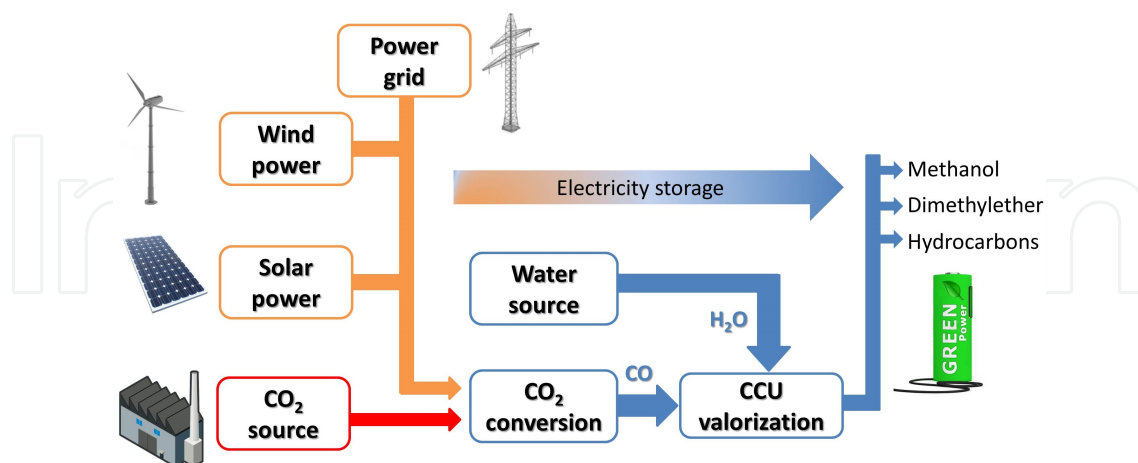

Figure 1. Generic and idealized energy cycle using captured CO$_2$ and H$_2$O to yield value-added products via renewable electricity.

Another important strategy that can be used to produce syngas is the dry reforming of CO$_2$ with methane. This alternative is also particularly attractive since it converts two of the principal gases responsible for the greenhouse effect. In spite of many advantages related to these approaches, there are, however, some critical issues that need to be addressed. In particular, it has to be noted that most of the CCU routes are associated to highly endothermic reactions (e.g., CO$_2$ conversion in Figure 1). Under classical industrial conditions (e.g., using a typical reactor configuration with packed bed tubes inside a furnace), these reactions are sustained and limited by the rate of heat transfer. This leads to high production costs, which turns the whole conversion chain economically unreasonable [8]. In order to overcome this problem, there is one technology worth investigating: plasma-assisted decomposition. Plasmas provide an ideal environment for CO$_2$ conversion due to the formation of high energetic charged species that can initiate chemical reactions difficult or impossible to obtain using ordinary thermal mechanisms. In particular, plasma electrons can lead to the formation of vibrationally excited molecules, which are able to dissociate through the vibrational ladder-climbing process [9]. Among different types of plasmas that can be used for CO$_2$ decomposition, the so-called cold (also known as nonthermal) plasmas are the most promising candidates. These electrical discharges are characterized by nonequilibrium conditions, under which electrons, ions, and neutral species have different translational and – in case of molecules – internal (ro-vibrational) energies. This results in formation of specific nonequilibrium gaseous media in which endothermic processes with increased energy efficiencies and dissociation rates can be achieved [9].

1.2. The CO$_2$ dissociation in cold plasma

From a practical point of view, all the research involving CO$_2$ conversion in cold plasmas has one common task: increasing the energy efficiency associated to the decomposition process while keeping the dissociation rate at a reasonably high level. For the sake of comparison between different experiments, the energy efficiency rate (η) of the CO$_2$ decomposition is

usually defined as the ratio of the CO_2 dissociation enthalpy (ΔH) and the injected energy per CO molecule produced in the plasma (E_{CO}):
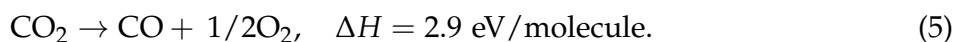
$$\eta = \Delta H / E_{CO}. \tag{2}$$

Note that ΔH depends on reaction mechanism. The most desirable chemical route to produce CO from CO_2 would be a process or a sequence of processes requiring the smallest amount of energy. In the most direct way, the CO_2 decomposition occurs via:

$$CO_2 \rightarrow CO + O, \quad \Delta H = 5.5 \text{ eV/molecule.} \tag{3}$$

The atomic oxygen created is able then to react either with another oxygen atoms to form O_2 or with vibrationally excited CO_2 (denoted as CO_2^*) according to [9]:

$$O + CO_2^* \rightarrow CO + O_2, \quad \Delta H = 0.3 \text{ eV/molecule.} \tag{4}$$
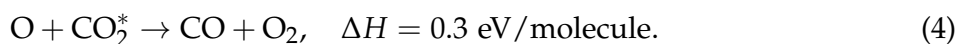
Combining the above equations, the net reaction for the total dissociation process of one CO_2 molecule yields

$$CO_2 \rightarrow CO + 1/2O_2, \quad \Delta H = 2.9 \text{ eV/molecule.} \tag{5}$$

The energy efficiency rate given by Eq. 2 can be rewritten for the total CO_2 decomposition η (%) according to

$$\eta = \frac{\chi \cdot 2.9}{E_m}, \tag{6}$$

where χ (%) is the CO_2 dissociation rate, while E_m is the specific energy input (in eV/molecule and defined as the ratio of the discharge power over the gas flow rate through the discharge). It is important to stress that in practice, there are many chemical and system inefficiencies (e.g., reverse reactions forming back CO_2) that contribute to a non-efficient decomposition. In this context, the ideal scenario is to find the type of discharge with optimal plasma properties (pressure, flow rate, power, etc.) that minimize these unwanted mechanisms. The most common types of plasma discharges used for CO_2 conversion include the radio frequency (RF) [10], dielectric barrier discharge (DBD) [11–15], gliding arc plasmatron (GAP) [16, 17], glow discharge (GD) [18], and microwave (MW) [9, 19, 20] (see Table 1).

It is interesting to note that among different plasma sources used nowadays, DBD is probably the most widely used in CO_2 conversion research. Although the efficiencies obtained with this source are typically low, the possibility to work at atmospheric pressure under nonequilibrium conditions is very promising. Combined with a catalytic material, these discharges should also improve the selective production of the targeted compounds [15]. In addition, the DBD has a very simple design, which is beneficial for upscaling in industrial applications.

Plasma (f_d)	Power (W)	Pressure (Torr)	E_m (eV/mol)	η(%)	Ref.
RF (13.56 MHz)	~10	0.05–0.3	~39	~ 3	[10]
DBD (0–30 kHz)	~10	760 (1 atm)	~0.2	~ 2	[11]
DBD (6–75 kHz)	80	760 (1 atm)	~2.0	~8	[12]
DBD (1–30 kHz)	45	760 (1 atm)	~5.7	~3.3	[13]
DBD (30–90 kHz)	200	760 (1 atm)	~13.9	~2.0	[14]
DBD (60–130 kHz)	5–80	760 (1 atm)	~0.1-10	<5	[15]
GAP (20 kHz)	~200	760 (1 atm)	~2.0	~30	[16]
GAP (n/a)	n/a	760 (1 atm)	~0.3	~43	[17]
GD (8.1 kHz)	~20	760 (1 atm)	~4.0	~7	[18]
MW (2.45 GHz)	1200	760 (1 atm)	~5.0	~20	[19]
MW (2.45 GHz)	n/a	120	~0.3	~85	[9]
MW (0.91 GHz)	1000	90	~1.9	~35	†

Table 1. List of various plasma sources (excited at frequency f_d) used to decompose CO$_2$ and the corresponding energy efficiencies. † refers to this work

On the other hand, the GAPs have also been receiving a special attention in environmental applications because they can operate at atmospheric pressures while reaching relatively high efficiencies [21]. Nunnally et al. [17] have recently reported a maximum energy efficiency of 43% on CO$_2$ decomposition. This result was attributed to the reverse vortex flow configuration (also known as *tornado* effect) which increases the residence time of the plasma species and leads to a more uniform gas treatment.

Finally, the MW plasma sources are the ones that (until today) were able to provide the highest efficiencies (~85%) for CO$_2$ conversion (see Table 1). As pointed out by Fridman [9], the ability to create a strong nonequilibrium environment in MWs leads to the formation of vibrationally excited CO$_2$ states via vibrational-vibrational (VV) exchange reactions, which favors efficient dissociation. It has to be noted, however, that high energy efficiencies in MWs are usually achieved at reduced pressures (~100–200 Torr), which is not desirable for industrial purposes. Furthermore, MWs operating in the atmospheric regime seem to lead to a clear reduction in the energy efficiency (~20%) as recently reported by Spencer et al. [19]. This is due to the fact that the degree of nonequilibrium tends to decrease at higher pressure in these discharges. Nevertheless, these considerations make the abovementioned discharges particularly attractive to investigate and to further develop toward an industrial implementation.

1.3. The research strategy used

The current study is based on the project P07/34 "Plasma-Surface Interaction" of the Interuniversity Attraction Poles (IAP) action supported by the Belgian Science Policy Office (BELSPO), which (among other subjects) combines experimental and theoretical activities related to CO$_2$ decomposition. The research was focused on the systematic investigation of the basic plasma parameters in microwave discharges aiming at enhancing our understanding on the CO$_2$ decomposition process. The characterization of the discharge has been done through different diagnostic methods, namely, optical emission spectroscopy (OES), two-photon absorption laser-induced fluorescence (TALIF), and gas chromatography

(GC). Due to their nonintrusiveness, these techniques are particularly useful to characterize the CO_2 decomposition in the microwave discharge domain. In this context, we explore the mentioned diagnostic techniques either directly or via development of the additional easy-to-handle tools which, at the same time, may be particularly valuable for maximization of the energy efficiency in real cold plasma discharges targeted to the CO_2 conversion. Among different important parameters investigated, a special attention was given to the measurement of the (i) space-resolved CO_2 dissociation rate, (ii) gas temperature, and (iii) density of products at the end of the reactor exhaust (post-discharge).

2. The experimental part

The plasma investigated in this work was created and sustained through microwave surfaguide-type wave discharges (here abbreviated as MSGDs). This particular kind of microwave plasma source was already proven to be very efficient to produce atomic species in the discharge volume [22]. Working in the pulsed regime, the MSGDs ensure even more efficient molecular dissociation of diatomic or multi-atomic species [23]. The schematic representation of the experimental setup is shown in Figure 2. Two MSGDs excited at different frequencies of 2.45 and 0.915 GHz have been involved in this work. In either case, the discharge was sustained inside a quartz tube (inner radius $R = 7$ mm and length $L = 30$ cm) surrounded by another (polycarbonate) tube for cooling purposes. The mentioned cooling has been performed using an oil flow of 10 °C. The gas mixture was injected from the top of the system and regulated by the electronic mass flow controllers. The pressure range studied was varied from 1 to 90 Torr. The core system was always surrounded by a grounded aluminum grid to prevent a leak of the microwave radiation into the outer space (not shown in Figure 2). The power supply was able to create discrete pulses, typically with lengths in the order of milliseconds to microseconds. A more detailed description of the MSGD can be found in [23]. In respect to the plasma characterization, the OES measurements were performed along the discharge axis, while the TALIF and GC methods were implemented in the post-discharge of the reactor (see Figure 2). The particularities of each diagnostic along with the investigated parameters are described below.

2.1. OES implementation

OES represents a powerful yet nonintrusive characterization technique based on the measurement and analysis of the light emitted from spontaneous relaxation of excited species in plasma. In the current work, the OES was implemented in the 2.45 GHz MSGD system through an Andor Shamrock-750 spectrometer and an Andor iStarDH740-18F-03 ICCD camera with a built-in digital delay generator. In a first approximation (considering an optically thin plasma), the observed line intensity $I(p,q)$ of a particular electronic transition $n(p) \rightarrow n(q)$ is defined as (see, e.g., [24])

$$I(p,q) = h\nu_{pq}(4\pi)^{-1}n(p)A(p,q)L, \tag{7}$$

where $h\nu_{pq}$ is the energy gap between the upper and lower level p and q, $n(p)$ the density of the emitting level, $A(p,q)$ the radiative transition probability, and L the line segment of the plasma along which radiation is collected. A typical emission spectrum recorded at the top of the discharge ($Z = 7$ cm in Figure 2) in a pure CO_2 plasma is shown in Figure 3. As one
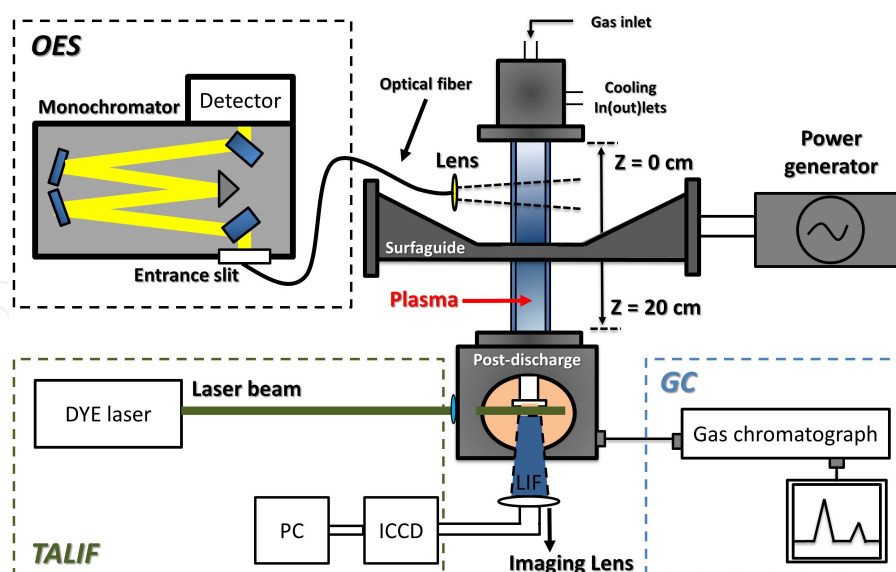
Figure 2. Schematic representation of the MSGD together with the diagnostics techniques used for the plasma characterization.

can see, the Angstrom system ($B^1\Sigma \to A^1\Pi$) of CO occupies the larger part of the spectrum ($\sim$400–700 nm), neighboring the CO third positive system ($b^3\Sigma^+ \to a^3\Pi_r$) [25]. Other CO bands (e.g., triplet, Herman, and Asundi [25]) were not identified during the measurements, and their contribution is accepted to be negligible for further analysis. The presence of the CO$_2^+$ ultraviolet doublet ($B^2\Sigma^+ \to X^2\Pi$) emission at 289 nm and the atomic O peaks in the near-infrared (NIR) part of the spectrum were identified as well. The continuum part of the spectrum induced by CO–O recombination with a maximum at $\sim$450 nm is also visible. It is interesting to note that neither C$_2$ nor C emission has been observed in this work, which suggests a negligible amount of atomic carbon produced.
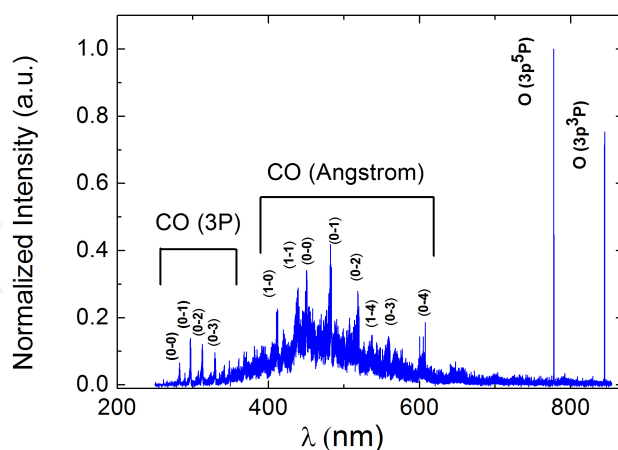

Figure 3. Appearance of the emission spectrum of a pure CO$_2$ microwave discharge acquired at $Z = 7$ cm. The notation (v'-v'') refers to the vibrational transition, where v'($''$) stands for upper (lower) vibrational energy level. Reproduced with permission from Ref. [20]. Copyright 2014 IOP Publishing.

The parameters investigated by OES in the plasma phase were the (i) rotational temperature (T_{rot}) and (ii) space-resolved CO$_2$ dissociation rate $\chi(Z)$. OES can be used to determine T_{rot},

provided there is access to a suitable rotational emission band (I_{rot}). In case of Boltzmann equilibrium among the rotational levels, the T_{rot} can be determined via [26]

$$I_{rot} = \frac{C}{Q_R} \frac{1}{\lambda^4} S_J \cdot Exp\left(- \frac{F(J')hc}{k_B T_{rot}} \right) \tag{8}$$

where C is a constant combining all the terms nondependent on the rotational number J, Q_R the rotational state sum, λ the wavelength of the emitted radiation, S_J the J-dependent dimensionless Honl-London factors, $F(J')$ the rotational energy term ($J'('')$ stands for upper (lower) rotational level), k_B the Boltzmann constant, and c the speed of light. Based on Eq. 8, the so-called Boltzmann plot in the coordinates ($F(J')$, $Log(I_{rot}/S_J)$) is often applied to extract the T_{rot}. This parameter is particularly relevant in CO_2 plasmas since it gives a first estimation of the gas temperature T_{gas} [20]. In the current work, the rotational spectra of CO and N_2 have been used for rotational analysis. The Honl-London factors of these molecules can be found in [26].

On the other hand, the estimation of the $\chi(Z)$ cannot be directly obtained from the emission intensity since the number densities of the decomposed species are represented by their non-radiative ground states. The simplest way to overcome this issue by OES is through the so-called *corona* model [27] and the actinometry technique (proposed by Coburn and Chen [28]). Briefly speaking, the corona model assumes that upward transitions (forming excited species) are only due to electron collisions from the ground state, while downward transitions occur via radiative decay. Under these assumptions, the creation-loss balance for the upper level p can be written according to

$$n_g n_e k(g,p) = n(p) \sum_q A(p,q) \tag{9}$$

where n_g is the ground state density, n_e the electron density, $k(g,p)$ the rate coefficient of excitation from the ground level, and $\sum_q A(p,q)$ the sum of all radiative de-excitation processes with origin in the p level. In order to get quantitative information about the prospected n_g, the actinometry technique is applied. In this procedure, a small amount of gas (actinometer) with known concentration n_g^{act} and line intensity $I(i,j)$ with transition $n(i) \to n(j)$ is added into the discharge. From the ratio of both emission intensities $I(p,q)$ and $I(i,j)$ and combination between Eqs. 7 and 9, the following expression can be deduced:

$$n_g = n_g^{act} \frac{I(p,q)\nu_{ij}A(i,j)k(g,i)\sum_q A(p,q)}{I(i,j)\nu_{pq}A(p,q)k(g,p)\sum_j A(i,j)}. \tag{10}$$

In the current research, the actinometry was used to measure the density of CO in the discharge, which leads to the $\chi(Z)$ provided that the initial CO_2 density is known. A small amount (5%) of N_2 was chosen as actinometer due to the proximity of the $N_2(C^3\Pi_u)$ (11.05 eV) and $CO(B^1\Sigma^+)$ (10.78 eV) excited states. Due to this proximity, the populations of these two energetic states should correlate as a result of the electron excitation. The emission lines chosen for the actinometry analysis correspond to the transitions $CO(B^1\Sigma^+)(v' = 0) \to CO(A^1\Pi)(v'' = 1)$ and $N_2(C^3\Pi_u)(v' = 0) \to N_2(B^3\Pi_g)(v'' = 2)$, from the Angstrom system of CO and second positive system (SPS) of N_2, respectively. A negligible dissociation rate of

N$_2$ was assumed. This last point is supported by (i) OES measurements in CO$_2$-5%N$_2$ gas mixtures showing a negligible emission of atomic nitrogen [20] and (ii) CO$_2$-N$_2$ modeling data showing a negligible N$_2$ dissociation at low N$_2$ admixtures [29]. The rate coefficients necessary in Eq. 10 were calculated via the Maxwellian distribution (assuming electron temperature $T_e \sim 1$ eV as measured in [20]) and the excitation cross sections of CO [30] and N$_2$ [31]. Finally, it is important to mention that Eq. 10 is only valid in CO$_2$ low-pressure discharges with negligible excitation out of metastable levels (e.g., CO($a^3\Pi_r$) and N$_2$($A^3\Sigma_u^+$)). An extended collisional-radiative model would be required in the high-pressure regime, since the excitation out of these intermediate levels is expected to play an important role as well (see, e.g., [32]).

2.2. TALIF implementation

Laser-based plasma diagnostic techniques have largely contributed to understanding plasma kinetics since the 1970s with the development of solid-state lasers [33]. One of these techniques is the TALIF, which is based on the measurement of the excited state fluorescence radiation induced by the excitation of the ground state via resonant absorption of laser photons. The fluorescence signal is proportional to the laser intensity thus allowing detection of the ground state population density. The use of two laser photons is required for most light atoms because the energy gap between the lower and the first electronic excited level exceeds the laser energy produced by conventional dye lasers.

In the current work, the TALIF was applied in the post-discharge region of the 2.45 GHz system through a YAG:Nd pumping laser (Spectra Physics INDI YAG) coupled with a Sirah Cobra Stretch dye laser. The TALIF signal was acquired perpendicularly to the laser beam through an ICCD detector coupled with Nikkor 50 mm lens (see Figure 2). The parameter investigated by TALIF was the oxygen ground state O($^3P_2$) density. The excitation of this level was performed via 2×225.586 nm laser photons, while the fluorescence was measured through the radiative decay of the O(^{3}S) level at 844.68 nm. An illustration of the actual fluorescence signal is shown in Figure 4. It is important to stress that the data obtained here by TALIF only yields relative densities. In order to achieve absolute results, the induced fluorescence needs to be calibrated (normally via noble gases [34]). Even though such absolute measurements are particularly promising to improve our understanding on the role played by the oxygen atoms in CO$_2$ discharges, they were not covered by the current study.

2.3. GC implementation

GC offers a sensitive detection of stable reaction products at the exhaust of the plasma reactor. These products are separated inside the gas chromatograph due to their distribution between two non-mixable phases: a stationary phase (solid and/or liquid, filled in the so-called separation column) and the mobile phase (carrier gas, flowing through the column and containing the gaseous sample mixture) [35]. Nowadays, the GC is often applied in many kinds of CO$_2$-containing discharges, including CO$_2$–N$_2$ [29], CO$_2$–H$_2$O [36], CO$_2$–CH$_4$ [37], CO$_2$–Ar [38], etc.

In the current work, the gas chromatograph (Bruker) equipped with a carbon molecular sieve column and a molecular sieve 5A column in series connected with a thermal conductivity detector was implemented in the post-discharge of the 0.91 GHz system. As this plasma
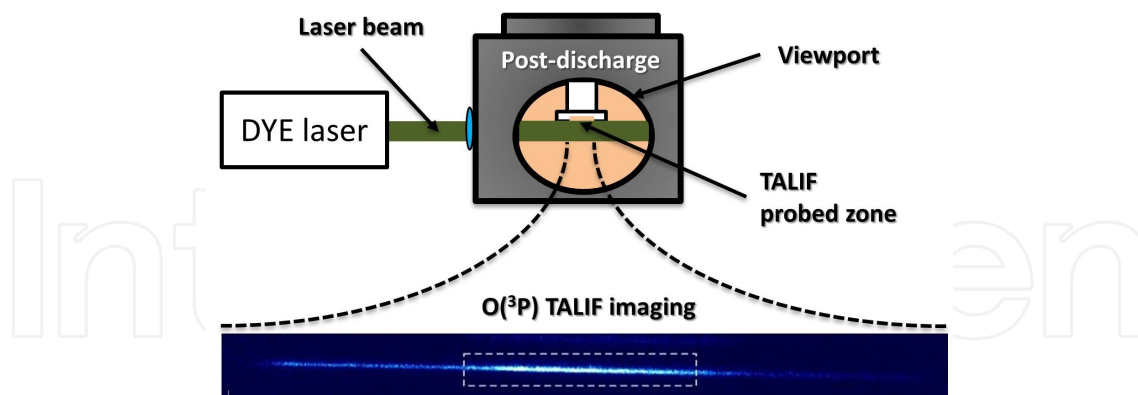
Figure 4. Schematic of the post-discharge region (above), along with the actual $O(^3P_2)$ image kept by the ICCD detector (below). Dashed rectangle represents the TALIF signal integration area.

source worked in reduced pressure regime, a sampling system was developed between the post-discharge and the gas chromatograph. The low-pressure sample coming from the post-discharge is diluted with neutral gas, in order to reach atmospheric pressure, prior to its injection in the chromatograph. Argon was used as a carrier gas. The CO_2 dissociation rate is calculated by

$$\chi = \frac{A_{CO_2}^{off} - A_{CO_2}^{on}}{A_{CO_2}^{off}}, \tag{11}$$

where $A_{CO_2}^{on}$ $(A_{CO_2}^{off})$ is the chromatograph signal of CO_2 when the plasma is switched on (off). It is important to emphasize that unlike OES, the GC does not provide *in situ* data. However, GC is advantageous over the actinometry method above-described since its applicability is not dependent on the discharge pressure and the accuracy of any population model.

3. The characterization of the discharge area

In this section, we will discuss the results related to investigation of the pulsed CO_2-containing discharges by OES. The energy delivered in the plasma pulse (E_p) during these measurements was varied from 0.8 J to about 1.2 J. The discharge pressure was kept below 5 Torr in this part of work.

3.1. Spatial analysis (OES)

The first insight that one can take regarding the plasma composition is based on the discharge color. For instance, as reported by Timmermans et al. [39], the emission of C_2 molecules in CO_2 discharges (only detected at high pressures due to the significant production of atomic carbon) is represented by a typical green emission. On the contrary, in our case, the light emission from the discharge always showed a strong blue emission due to the presence of CO

(see Figure 5). Furthermore, an increase of this light (readily observed by eye), after passing the waveguide (bottom part in this case), has motivated the space-resolved measurements along the discharge tube. Being represented at two different positions in the discharge (top and bottom), the emission spectrum shows certain changes reflecting the molecular decomposition process happening along the gas flow direction (see Figure 5). In addition, one can clearly observe a definite increase of CO Angstrom emission intensity from the top to the bottom of the tube.
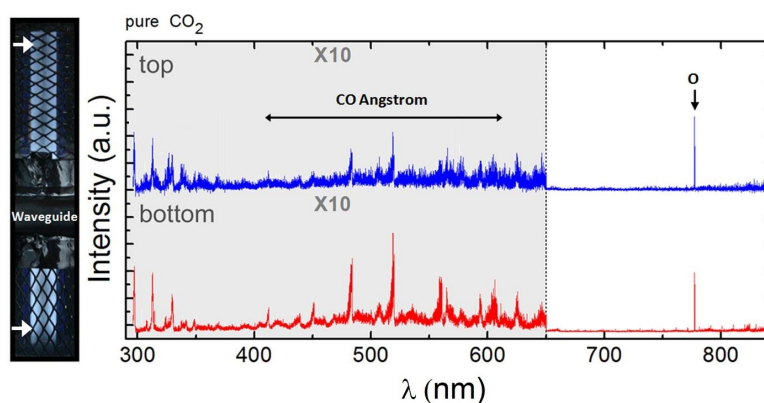
Figure 5. Emission spectra of the CO$_2$ MSGD taken at two different discharge positions (shown by the white arrows). Pressure ~3 Torr.

The abovementioned spatial increase of CO emission is also visible via time-resolved OES imaging (see Figure 6). These measurements provide a density mapping of the excited species in plasma. A filter that passes wavelengths within the 480 nm range was used as indicator of the CO Angstrom emission. Using a plasma on-time of 600 μs, one can clearly see that the CO emission extends axially along the quartz tube with clear predominance at the bottom region of the discharge.
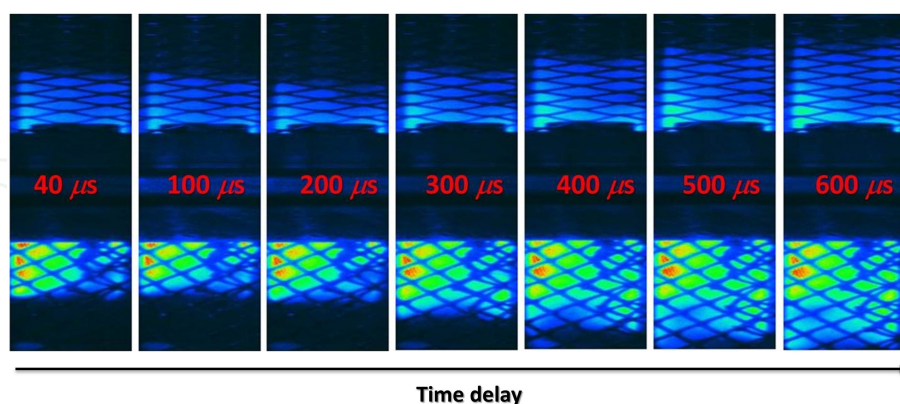

Figure 6. Time-resolved two-dimensional OES imaging of the CO$_2$ MSGD using a 480 nm optical band-pass filter. The iCCD camera was positioned ~15 cm away from the surfaguide. The mean power applied was 300 W with plasma on-time of 600 μs and 50% duty cycle. Each frame is a single-shot picture with a gate step of 20 μs.

In order to clarify the previous observations, the space-resolved temperature measurements were performed. Figure 7 shows T_{gas} calculated via the Boltzmann plot (as described in

Section 2.1) through the CO and N_2 rotational bands. The given error bars correspond to the statistical errors of the Boltzmann fitting in each case. Note that the space interval $Z \approx 8$–13 cm was inaccessible for optical measurements due to the presence of the waveguide. These measurements suggest a linear increase of T_{gas} along the gas flow direction. The results can be interpreted as a trace of the CO_2 decomposition process. Indeed, if the CO_2 molecules in plasma undergo dissociation along the discharge tube, the collision rate increases toward the gas flow direction, which may explain the observed temperature increase. A possible enhancement of the vibrational energy exchange in the plasma phase may also induce vibrational-translational (VT) exchange, which leads to an increase of the gas heating.
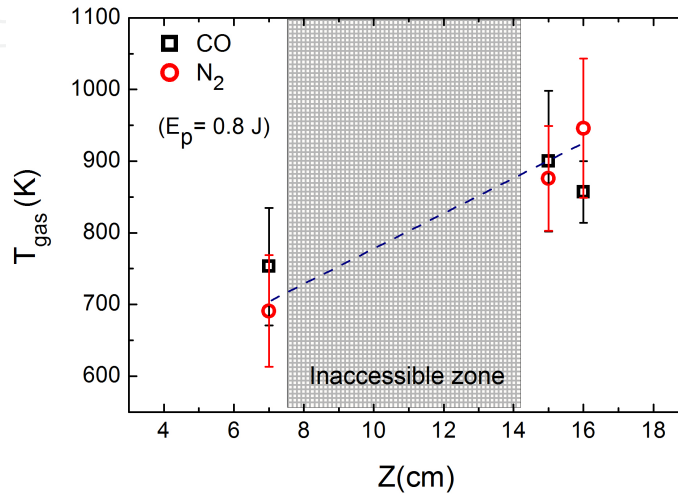

Figure 7. T_{gas} determined based on the N_2 and CO rotational temperatures at different positions of the discharge tube. The $CO_2 + 5\%N_2$ gas mixture is used with pulse (period) of $1.0\,(1.5)$ ms. Adapted with permission from Ref. [20]. Copyright 2014 IOP Publishing.

3.2. CO_2 dissociation rate (actinometry)

The investigation related to the CO_2 dissociation rate obtained by the actinometry method (described in Section 2.1) is presented in this section. The $CO_2 + 5\%N_2$ gas mixture with pulse (period) of $1.0\,(1.5)$ ms was used. The actinometry ratio between CO and N_2 was acquired 0.7 ms after the beginning of the plasma pulse in order to ensure a steady-state plasma regime. As a result of our measurements, a nonuniform $\chi(Z)$ along the gas flow direction was found, as illustrated in Figure 8. The experimental points of $\chi(Z)$ at the top of the discharge are well described by a linear fit (see Figure 8). However, the strong increase (almost four times) between the extremities of the discharge suggests a fast evolution of $\chi(Z)$ in the waveguide vicinity. To fit the obtained $\chi(Z)$ data, the so-called logistic growth has been proposed:

$$\chi(Z) = \chi_0 + \frac{\chi_{max}}{1 + e^{-r(Z-Z_c)}}, \qquad (12)$$

where χ_0 (%), Z_c (cm), and χ_{max} (%) are the initial values of the dissociation rate, the middle position of the discharge, and the maximum value of dissociation rate (defined as an average value at the end of the tube). The r (cm^{-1}) is the free fit parameter (see Figure 8). A symmetrical power distribution in the discharge is assumed in this case: $\chi\,(Z=Z_c) \sim$

$\chi_{max}/2$. A derivative of Eq. 12 should correspond to the spatial distribution of the power absorbed in the plasma bulk P_{abs} which is used for CO$_2$ decomposition. Such a distribution can be characterized by the correspondent width (FWHM), i.e., a spatial region where the decomposition is most efficient, as shown in Figure 8, where the red curve represents the derivative of the black one. As one can see, the initial increase of P_{abs} coincides with a small experimental increase of $\chi(Z)$ at the beginning of the discharge ($Z = 4$–7 cm), followed by the fast growth of $\chi(Z)$ in the waveguide region where P_{abs} is supposed to be maximum.
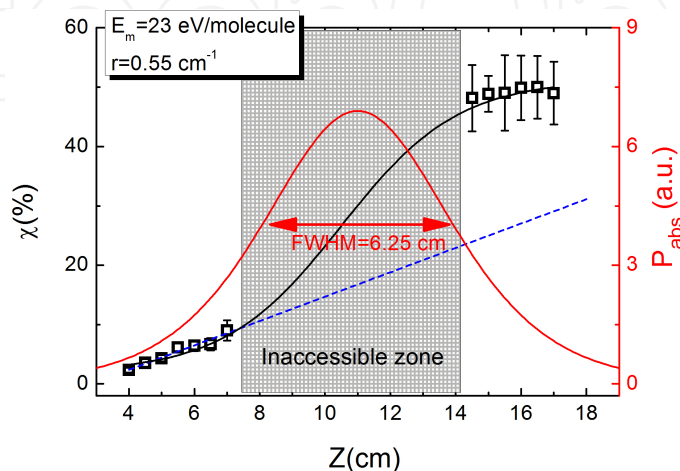

Figure 8. Space-resolved values of the dissociation rate χ (left scale) and the power absorbed in the plasma bulk P_{abs} (right scale) measured at $E_m = 23$ eV/molecule. Reproduced with permission from Ref. [20]. Copyright 2014 IOP Publishing.

Furthermore, it was verified that $\chi(Z)$ increases with E_m as shown in Figure 9. It is interesting to note that our measurements show that $\chi(Z)$ likely reaches a steady state at the bottom of the discharge, whereas a definite linear increase in $\chi(Z)$ is always recognized at its top, i.e., before the gas passes the waveguide. Such differences can be associated with the different chemical processes between these two discharge regions, which should be strongly related to the different power absorption channels. It would be interesting to compare these results with those obtained in an extended discharge tube in order to further investigate this last point.

A linear proportionality between the χ_{max} and E_m is also observed in our case, as shown in Figure 10. A similar behavior of the CO$_2$ decomposition rate which grows linearly when increasing the power and/or decreasing the flow rate is found in [40]. At the same time, based on Eq. 6, η is found to be $\sim$6% at different E_m (see Figure 10).

3.3. Gas temperature analysis (line ratio)

The study of T_{gas} via the CO rotational band was further investigated in order to (i) validate the Boltzmann plot results previously obtained and (ii) search for a simple gas temperature formula based on CO spectral synthesis. Figure 11 shows an example of the so-calculated $CO(B^1\Sigma)(v' = 0) \rightarrow CO(A^1\Pi)(v'' = 1)$ transition based on Eq. 8. The final theoretical spectrum includes the sum of the different rotational branches (P, Q, R corresponding to $\Delta J = J' - J'' = -1, 0, +1$). To reflect the broadening of the spectral lines, a pseudo-Voigt distribution [41], i.e., a combination of a Gaussian and a Lorentzian function, is used:
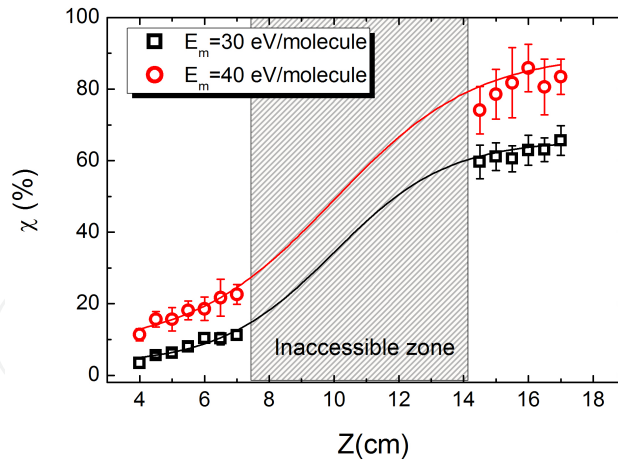
Figure 9. Space-resolved measurements of the CO_2 dissociation rate χ for two different E_m values. The region between about 8 and 14 cm was not optically accessible. Reproduced with permission from Ref. [20]. Copyright 2014 IOP Publishing.
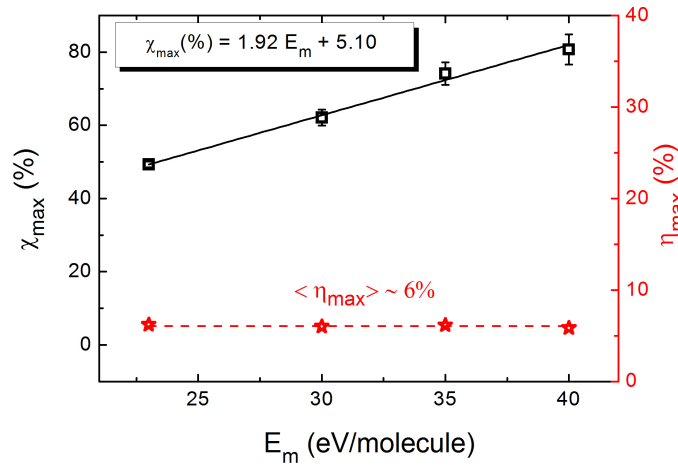

Figure 10. Maximum CO_2 dissociation rate χ_{max} (left scale) along with its energetic efficiency η_{max} (right scale) as a function of E_m. Reproduced with permission from Ref. [20]. Copyright 2014 IOP Publishing.

$$g(p, w_G, w_L) = p \cdot Exp[-4Log(2)(\frac{\lambda - \lambda_0}{w_G})^2] + (1-p)\frac{w_L}{w_L^2 + 4(\lambda - \lambda_0)^2}, \qquad (13)$$

where p is the contribution of the Gaussian function, λ_0 the line central wavelength, and w_G and w_L the full width at half-maximum (FWHM) for the Gaussian and Lorentzian profiles, respectively. The Voigt profile parameters were experimentally determined by measuring the shape of the 435.8 nm Hg line ($^3P_1$–$^3S_1$) from an Ar-Hg lamp (see Figure 11). The Hg line chosen for determination of the monochromator apparatus function is assumed to have (i) a spectral response similar to the one of the CO spectra and (ii) Doppler, Stark, and van der Waals broadening much smaller than the instrumental broadening [42–44]. The rotational peaks located at $P_1 = 481.61$ and $P_2 = 482.48$ nm were chosen in order to build a line-ratio formula. In this procedure, special attention was paid to find isolated peaks with good visibility and good sensitivity to the gas temperature, as discussed in [45]. To avoid bulky calculations, the expression for T_{gas} is then derived, taking into account the contribution of all
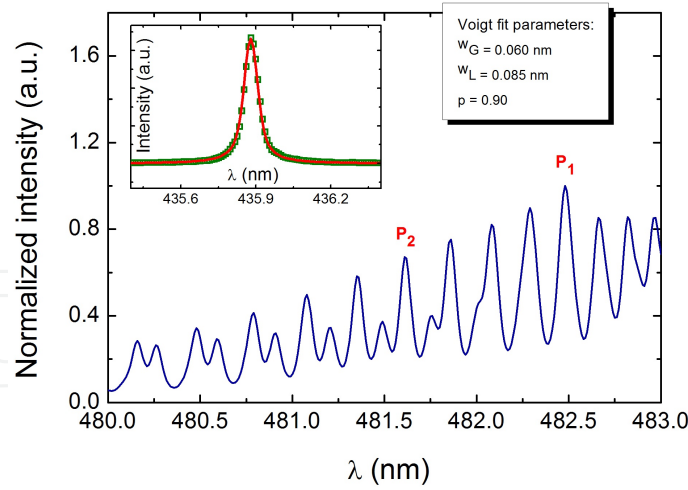
Figure 11. Synthetic spectrum of the molecular transition from the CO Angstrom rotational band calculated at $T_{rot} = 470$ K. Inset: measured Hg (435.8 nm) emission line (squares) and the corresponding fit (solid line) using a pseudo-Voigt function given by Eq. 13. Reproduced with permission from Ref. [41]. Copyright 2014 OAS Publishing.

the P, Q, and R rotational branches based on a semi-analytical approach, namely, when the peak ratio is determined as a function of T_{gas} for each rotational spectrum synthesized. After linearization in the coordinates $(Log(R), 1/T_{gas})$, the final result for the mentioned peaks can be presented in the form:

$$T_{gas}(K) = 343(0.36 + Log(R))^{-1}, \tag{14}$$

where $R = P_1/P_2$ is the peak ratio. The graphical representation of Eq. 14 between 200 and 10 000 K (typical range of cold plasmas) is given in Figure 12. The relative error of the T_{gas} determination relatively to the accuracy of the line intensity ratio (δT_{gas}) can be determined after differentiating Eq. 14. As a result, we obtain
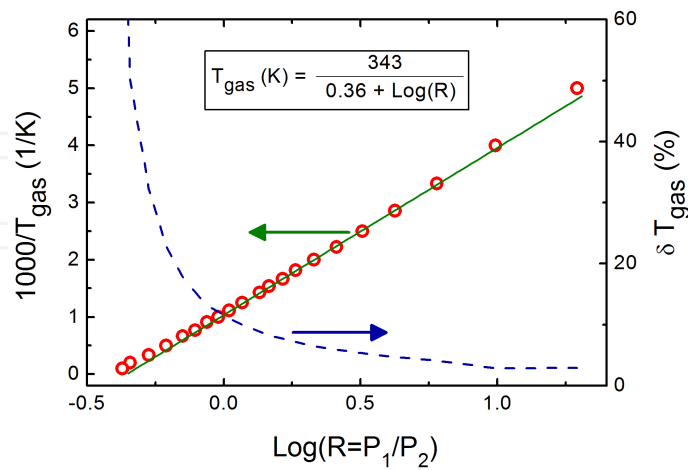

Figure 12. T_{gas} determination chart based on the line ratio between two spectral peaks in the CO Angstrom band (left scale). The red circles and the solid line represent the calculated points and the linear fit, respectively. The dashed line (right scale) indicates the relative error for the gas temperature – δT_{gas}. Reproduced with permission from Ref. [41]. Copyright 2014 OAS Publishing.

$$\delta T_{gas}(K) = \delta R \cdot (0.36 + Log(R))^{-1}. \tag{15}$$

The quantity δT_{gas} is given as a function of $Log(R)$ in Figure 12 where the R relative error $\delta R = 0.05$ is assumed. As we can see, the T_{gas} relative error increases dramatically, when $Log(R) < 0$, exceeding 30% for the temperatures above $\sim$3000 K. This fact limits the applicability of the proposed method at high gas temperatures.

In order to test the proposed method, the time-resolved T_{gas} was measured in pure CO_2 MSGD with a plasma pulse (period) of 1.0 (1.5) ms. The proposed line-ratio method is compared with the results obtained by the Boltzmann plot method and direct comparison between the measured and calculated spectra. Figure 13 shows a reasonable agreement in terms of T_{gas} evolution for these different approaches. The uncertainty (about 11% in saturation) of the obtained T_{gas} by the line-ratio method is still in the range of the errors described by Eq. 15 at $T_{gas} \sim 800$ K. These time-resolved measurements also show that, at a fixed E_p, the T_{gas} grows at the beginning of the pulse and saturates after about 0.4 ms. These effects were observed previously for the other gas mixtures in the same type of discharges [46]. First effect corresponds to the gas heating at the beginning of the plasma pulse, whereas the second one reflects the equilibrium between the gas heating and heat dissipation and may be related to VT relaxation processes, as suggested in [46].
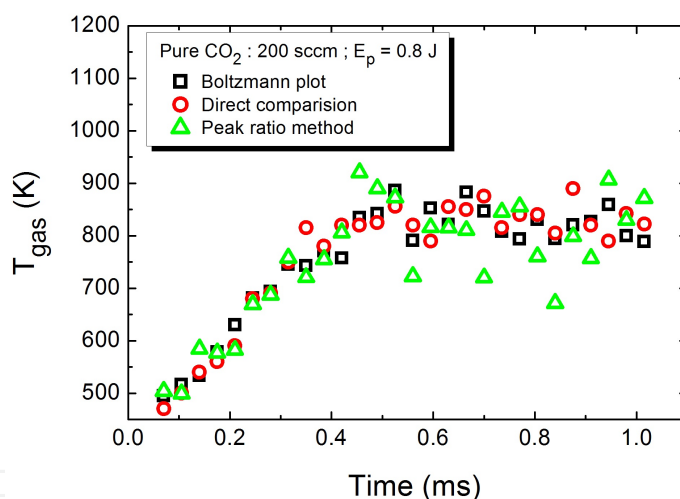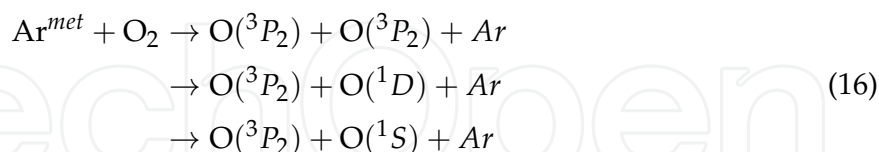

Figure 13. Time evolution of T_{gas} determined based on the CO rotational band using the Boltzmann method (black squares), direct spectral comparison (red circles), and proposed line-ratio method (green triangles). Reproduced with permission from Ref. [41]. Copyright 2014 OAS Publishing.

4. The characterization of the post-discharge area

The research related to the post-discharge area characterization of the microwave reactor is presented in this section. A special attention was devoted to the investigation of parameters that may favor the fine-tuning of CO_2 decomposition. This brings us to the study of the following effects: (i) Ar admixture, (ii) duty cycle, and (iii) discharge pressure. The motivation behind each effect, along with the results obtained, is presented below.

4.1. Ar admixture effect (TALIF)

The influence of Ar atoms in the chemistry of gas discharges containing oxygen species has been extensively studied over the past years (see, e.g., [47, 48]). In this context, it is well known that the Ar metastables (here denoted by Ar^{met}) play a key role as internal energy reservoirs for the production of atomic oxygen species via [48]:

$$\begin{aligned}
\mathrm{Ar}^{met} + \mathrm{O}_2 &\rightarrow \mathrm{O}(^3P_2) + \mathrm{O}(^3P_2) + Ar \\
&\rightarrow \mathrm{O}(^3P_2) + \mathrm{O}(^1D) + Ar \\
&\rightarrow \mathrm{O}(^3P_2) + \mathrm{O}(^1S) + Ar
\end{aligned} \qquad (16)$$

Furthermore, due to their long lifetime, the Ar^{met} may also contribute to the chemistry of the afterglow and post-discharges. These considerations have triggered the TALIF study on O($^3P_2$) formation as a function of the Ar admixture. The typical results related to the O($^3P_2$) density measurements in the Ar–O$_2$ and Ar–CO$_2$ mixtures are shown in Figure 14. Indeed, these measurements strongly suggest that Ar atoms enhance the O($^3P_2$) production. At low Ar admixtures, the strong molecular quenching induced by O$_2$/CO$_2$ should lead to a decrease in the Ar^{met} population and less O($^3P_2$) produced via Eq. 16. The last observation is supported by theoretical and experimental results obtained in Ar–O$_2$ [47] and Ar–CO$_2$ [49] MSGDs, which show a decrease of Ar^{met} (about three orders of magnitude) in the plasma phase as a consequence of the molecular quenching.
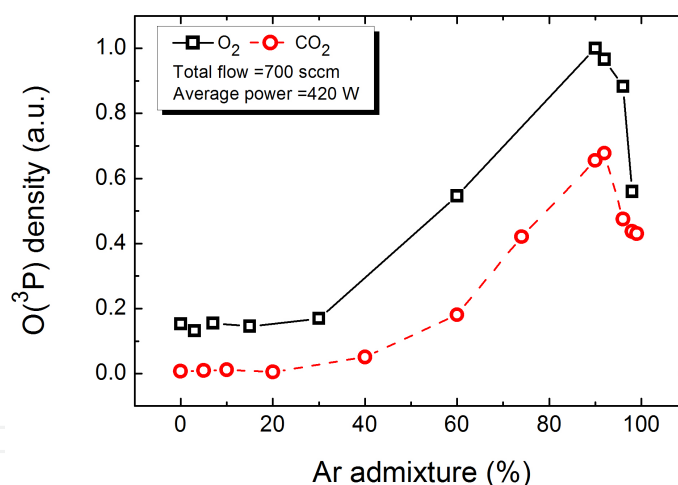

Figure 14. Density of the O($^3P_2$) as a function of the Ar admixture in O$_2$ (solid line) and CO$_2$ (dashed line) mixtures. The mean power applied was 400 W with a 0.7 kHz pulsing frequency and 33% duty cycle. The total gas flow in both mixtures was 700 sccm. The maximum Ar admixture used was 99%.

It is interesting to note that as the Ar content increases from ∼90% to 100%, there is a clear decrease of O($^3P_2$) as the source of oxygen (CO$_2$/O$_2$) is also decreasing. This leads to the formation of the maximum in O($^3P_2$) production around 90% of Ar admixture. Furthermore, it should be emphasized that the electron density is expected to decrease as the Ar admixture decreases since the power used for the production of electron-ion pairs is diverted into vibrational and rotational heating of the molecular gas. As a result of lower electron density, one might also expect a decrease in the contribution of the ladder-climbing processes (e.g., stepwise ionization) out of the Ar^{met}. These considerations (together with

low molecular quenching rate at low molecular admixture) may contribute to an increase of Ar^{met} population around 90% of Ar admixture. Further investigations are required in order to validate this last assumption, namely, the measurement of Ar^{met} densities in the post-discharge region of the reactor.

4.2. Duty cycle effect (TALIF)

The pulse discharge operation mode offers an additional feature that may increase the flexibility of the global dynamic plasma response in microwave discharges. In many experiments, the power interruption was usually found to be suitable for reducing gas heating in the discharge by injecting a large amount of power during the plasma on-time while keeping the average power at low values [23]. In case of microwave plasmas, this effect was already proven to be advantageous for the production of atomic nitrogen and oxygen in N_2 and O_2 discharges ([23, 50]).

In this work, the influence of the duty cycle (defined as the ratio between the plasma on-time and its repetition period) on the $O(^3P_2)$ production was investigated by TALIF (see Figure 15). These results clearly show an improvement in the $O(^3P_2)$ production as the duty cycle decreases. The CO_2-20% Ar gas mixture with a pulsing frequency of 0.5 kHz was used during these measurements.
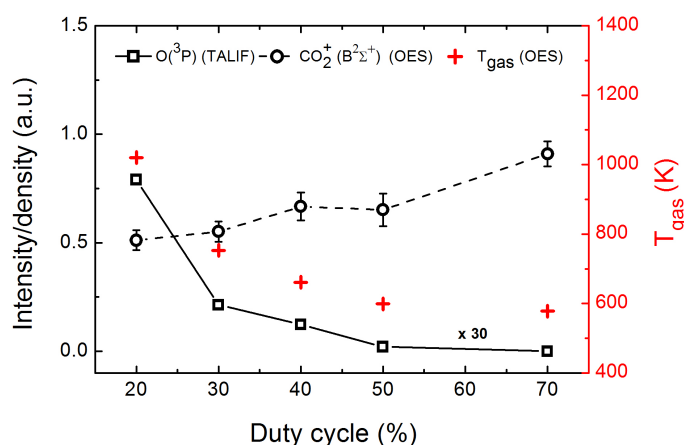

Figure 15. Left scale: Emission of CO_2^+ (dashed line) and density of $O(^3P_2)$ (solid line). The TALIF data was normalized to the maximum value obtained in Figure 14 and further multiplied by a factor of 30. Right scale: Gas temperature (crosses) calculated via Eq. 14. The mean power applied was 250 W with a 0.5 kHz pulsing frequency. The CO_2-20% gas mixture with total flow rate of 700 sccm was used.

It is important to stress that the average power was kept constant. On the other hand, by decreasing the power per pulse as the duty cycle increases, we found a decrease of T_{gas} (calculated via Eq. 14) that follows the $O(^3P_2)$ evolution. Interestingly, the emission of the ultraviolet doublet system of CO_2^+ (measured in the plasma phase by OES) shows an increase with the duty cycle. These observations suggest that low duty cycles favor the dissociative recombination of CO_2, which is responsible for the release of energy in the form of heating into the plasma [23]. There are other factors that may also play an important role in the power modulation effect, namely, the electron parameters and sources of internal energy (e.g., metastable species). For instance, as shown by the theoretical work of Subramonium et al. [51], it can be expected to find higher T_e values at the leading edge of the plasma on-time

as the duty cycle decreases. This result supports the data obtained, considering dissociation via electron impact of O$_2$ as the major source of O($^3P_2$).

4.3. Pressure effect (GC)

The pressure effect on the CO$_2$ decomposition was studied by GC (as described in Section 2.3) in this last part of the work. Figure 16 shows the χ (calculated via Eq. 11) and η (calculated via Eq. 6) evolution in the range of 20–90 Torr at different pulsing frequencies. The values obtained at low pressures are in good agreement with the theoretical calculations performed by Bogaerts et al. [52] for microwave plasmas sustained at 20 Torr. As the pressure increases, our experimental data clearly shows an improvement of the CO$_2$ decomposition with $\eta \sim 35\%$ and $\chi \sim 20\%$ at 90 Torr. Figure 16 also suggests that higher η values can be achieved with further increase of pressure. Unfortunately, such pressure range was limited by the current pumping system. As suggested by Fridman [9], these pressure-dependent results can be understood based on the increase of electron-neutral collision frequency in the plasma phase which favors the vibrational excitation of the asymmetric vibrational mode of CO$_2$ and leads to higher conversion rates. A possible decrease of T_e with the increase of discharge pressure might also enhance the vibrational excitation of CO$_2$ since less energy is wasted in electronic excitation. This last observation is supported by T_e measurements recently obtained in CO$_2$–Ar discharges [49]. However, further increase of pressure (eventually reaching the atmospheric range) may lead to higher VT relaxation rates, faster gas heating, and lower efficiencies. In this case, the plasma would act as a heater, which would bring additional problems such as the reverse reactions forming back CO$_2$.
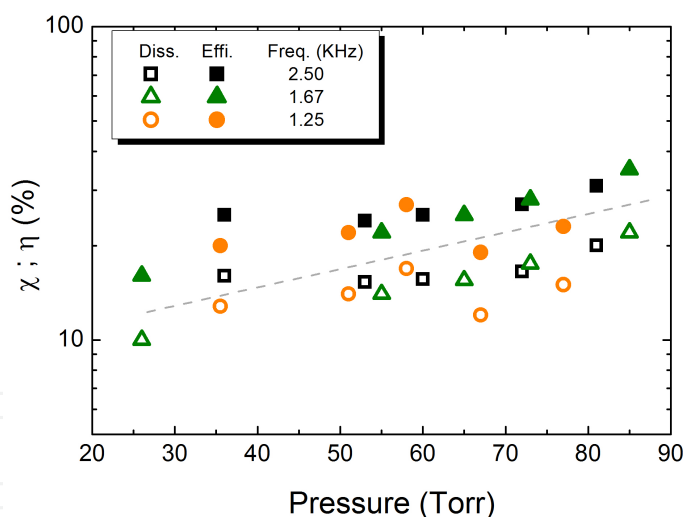

Figure 16. Evolution of the dissociation rate and energy efficiency of CO$_2$ as a function of the discharge pressure at different pulse frequencies. The mean power applied was 2000 W with 50% duty cycle. The flow of CO$_2$ was 15 slm ($E_m \approx 1.9$ eV/molecule).

5. Summary and conclusion

As new solutions to decrease our dependence on fossil fuels are required, the recycling of CO$_2$ into value-added materials may play a critical role in the near future. In this regard, plasma-assisted decomposition offers a practical and efficient way to convert CO$_2$

into valuable products that can be extremely useful in CCU applications. Therefore, and given the necessity to enhance the CO_2 conversion in plasma reactors, there is a constant need to improve the knowledge of CO_2-containing discharges through the development of experimental diagnostic techniques and the improvement of theoretical models. This chapter explores the microwave surfaguide discharge as one potential example of plasma technology that can be used for CO_2 conversion. In order to fully characterize our system and obtain a large set of valuable data, we used three different diagnostics: (i) optical emission spectroscopy, (ii) two-photon absorption laser-induced fluorescence, and (iii) gas chromatography. The first one is particularly useful to study the plasma region of the reactor, while the other two give an important insight on the density of products in the post-discharge region.

As a result of the optical emission spectroscopy measurements (via actinometry) along the discharge tube, a nonuniform distribution of the CO_2 dissociation rate is obtained in the gas propagation direction, which also depends on the specific energy input. This method offers a practical way to construct a CO_2 "dissociation map" through the discharge volume with the spatial resolution depending only on the collimating optics used in the optical emission measurements. With a proper population model to describe the excitation processes, such a mapping should give rather accurate results that may be particularly valuable for maximization of the CO_2 dissociation efficiency in cold plasma discharges.

A special attention has been also given to the measurement of the gas temperature, which is a fundamental parameter to characterize the dissipation of energy through gas heating. In this regard, a simple gas temperature formula based on the line ratio between two rotational peaks of the CO Angstrom rotational emission band was developed. This method is extremely useful if a quick gas temperature estimation without the spectral synthesis is required. It allows for T_{gas} determination, assuming the presence of CO emission from plasma discharge. The applicability of the proposed line-ratio formula is, however, limited by the temperature of about 3000 K, above which the measurement error is rather high (>30%). The validity of the proposed approach was additionally approved by the well-known Boltzmann plot, as well as by direct comparison with simulated spectra.

Concerning the post-discharge characterization, the research presented here was mainly focused on the study of parameters that may favor the fine-tuning of CO_2 decomposition. As a result of these measurements, the presence of Ar atoms was confirmed to be beneficial for the formation of the ground state atomic oxygen species. This effect was attributed to the high population density of Ar metastable species in the plasma phase at higher Ar admixtures. The gas mixture CO_2:Ar = 1:9 was found to be the most efficient proportion to produce the ground state atomic oxygen. On the other hand, the study of the power modulation effect also showed interesting results, namely, the increase of oxygen ground state species at lower duty cycle values. Finally, what is related to the pressure effect, a linear increase of CO_2 decomposition was obtained in the range of 20–90 Torr. The maximum value of energy efficiency obtained was about 35% with a reasonable dissociation rate of 20%. The complete set of results obtained in this work are summarized in Table 2.

Overall, the methods explored/developed in this work offer a valuable set of tools that can be applied in microwave and other plasma sources. In addition, the data presented here may also provide a useful input for modeling of the microwave surfaguide-type discharges operating under CO_2 gas mixtures. As a long-term perspective, the authors believe that

Parameter	Method	Result	Observation
Dissociation rate	Actinometry	↗ along the tube	Logistic growth
Energy efficiency	Actinometry	Constant at 6%	23–40 eV/mol.
Gas temperature	OES	↗ along the tube	Linear growth
Gas temperature	OES	↗ with plasma pulse	Satt. at ∼0.4 ms
Atomic oxygen	TALIF	↗ with Ar admixture	Max. at 90% Ar
Atomic oxygen	TALIF	↘ with duty cycles	T_{gas} dependent
Energy efficiency	GC	↗ with pressure	∼35% at 90 Torr
Dissociation rate	GC	↗ with pressure	∼20% at 90 Torr

Table 2. Summary of the various results obtained in this work and the corresponding methods used for the plasma characterization

microwave plasmas are among the most promising candidates to obtain an efficient CO_2 decomposition. However, further investigations related to understanding of the basic plasma processes are still required in the atmospheric pressure regime. The use of catalytic materials [15] (e.g., to improve selective production of decomposed products) and efficient discharge configurations (e.g., using a reverse vortex flow [17]) may turn out as the next step toward a practical implementation of microwave plasmas targeted for massive CO_2 conversion.

Acknowledgments

Author details

Tiago Silva[1]*, Nikolay Britun[1], Thomas Godfroid[2] and Rony Snyders[1,2]

*Address all correspondence to: tiago.dapontesilva@umons.ac.be

1 Chimie des Interactions Plasma-Surface (ChIPS), Universite de Mons, Mons, Belgium

2 Materia Nova Research Center, Mons, Belgium

References

[1] Shearer C, Bistline J, Inman M, Davis SJ. The effect of natural gas supply on US renewable energy and CO_2 emissions. *Environ. Res. Lett.* 2014; **9**:094008.

[2] Le Quiere C, et al. Global carbon budget. *Earth Syst. Sci. Data Discuss.* 2013; **6**:689–760.

[3] Trends in Atmospheric Carbon Dioxide [Internet]. 2015. Available from: http://www.esrl.noaa.gov/gmd/ccgg/trends/; accessed: 2015-08-15.

[4] Chen W. CO_2 conversion for syngas production in methane catalytic partial oxidation. *J. CO_2 Util.* 2014; **5**:1–9.

[5] Jiang Z, Xiao T, Kuznetsov VL, Edwards PP. Turning carbon dioxide into fuel. *Phil. Trans. R. Soc.* 2010; **368**:3343–3364.

[6] Centi G, Perathoner S. Opportunities and prospects in the chemical recycling of carbon dioxide to fuels. *Catal. Today.* 2009; **148**:191–205.

[7] De Falco M, Iaquaniello G, Centi G, editors. CO_2: A Valuable Source of Carbon. Springer, London/Heidelberg/New York/Dordrecht; 2013. 194p.

[8] Amouroux J, Cavadias S, Doubla A. Carbon dioxide reduction by non-equilibrium electrocatalysis plasma reactor. *IOP Conf. Series: Materials Science and Engineering.* 2011; **19**:012005.

[9] Fridman A. Plasma Chemistry. Cambridge University Press, New York; 2008. 978p.

[10] Spencer LF, Gallimore AD. Efficiency of CO_2 dissociation in a radio-frequency discharge. *Plasma Chem. Plasma Processes.* 2011;**31**:79–89.

[11] Lindon MA, Scime EE. CO_2 dissociation using the Versatile atmospheric dielectric barrier discharge experiment (VADER). *Front. Phys.* 2014; **2**:55

[12] Aerts R, Somers W, Bogaerts A. Carbon dioxide splitting in a dielectric barrier discharge plasma: a combined experimental and computational study. *ChemSusChem.* 2015; **8**:702–716.

[13] Ozkan A, Dufour t, Arnoult G, De Keyzer P, Bogaerts A, Reniers F. CO_2-CH_4 conversion and syngas formation at atmospheric pressure using a multi-electrode dielectric barrier discharge. *J. CO_2 Util.* 2015; **9**:74–81.

[14] Paulussen S, Verheyde B, Tu X, De Bie C, Martens T, Petrovic D, Bogaerts A, Sels B. Conversion of carbon dioxide to value-added chemicals in atmospheric pressure dielectric barrier discharges. *Plasma Sources Sci. Technol.* 2010; **19**:034015.

[15] Brehmer F, Welzel S, van de Sanden MCM, Engeln R. CO and byproduct formation during CO_2 reduction in dielectric barrier discharges. *J. Appl. Phys.* 2014; **116**:123303.

[16] Indarto A, Yang DR, Choi J, Lee H, Song HK. Gliding arc plasma processing of CO_2 conversion. *J. Hazard. Mater.* 2007; **146**:309–315.

[17] Nunnally T, Gutsol K, Rabinovich A, Rabinovich A, Gutsol A, Kemoun A. Dissociation of CO_2 in a low current gliding arc plasmatron. *J. Phys. D: Appl. Phys.* 2001; **44**:274009.

[18] Wang J, Xia G, Huang A, Suib SL, Hayashi Y, Matsumoto H. CO_2 decomposition using glow discharge plasmas. *J. Catal.* 1999; **185**:152–159.

[19] Spencer LF, Gallimore AD. CO_2 dissociation in an atmospheric pressure plasma/catalyst system: a study of efficiency. *Plasma Sources Sci. Technol.* 2013; **22**:015019.

[20] Silva T, Britun N, Godfroid T, Snyders R. Optical characterization of a microwave pulsed discharge used for dissociation of CO$_2$. *Plasma Sources Sci. Technol.* 2014; **39**:025009.

[21] Czernichowski A. Gliding arc: applications to engineering and environment control. *Pure Appl. Chem.* 1994; **66**:1301–1310.

[22] Ferreira CM, Moisan M, editors. Microwave Discharges: Fundamentas and Applications, Plenum Press, New York; 1993. 564p.

[23] Godfroid T, Dauchot JP, Hecq M. Atomic nitrogen source for reactive magnetron sputtering. *Chemical Surf. Coatings Technol.* 2003; **174–175**:1276–1281.

[24] Fujimoto T, Plasma Spectroscopy, Oxford: Clarendon Press; 2004. 304p.

[25] Pearse RWB, Gaydon AG. The Identification of Molecular Spectra. Wiley, New York; 1976. p. 407.

[26] Herzberg G, Molecular Spectra and Molecular Structure Vol 1: Spectra of Diatomic Molecules. Litton Educational Publishing, New York; 1950. 658p.

[27] Boffard JB, Lin CC, DeJoseph Jr. Application of excitation cross sections to optical plasma diagnostics. *J. Phys. D: Appl. Phys.* 2004; **37**;R143–R161

[28] Coburn JW, Chen M. Optical-emission spectroscopy of reactive plasmas – a method for correlating emission intensities to reactive particule density. *J. Appl. Phys.* 1980; **6**:3134–3136.

[29] Heijkers S, Snoeckx R, Kozak T, Silva T, Godfroid T, Britun N, Snyders R, Bogaerts A. CO$_2$ conversion in a microwave plasma reactor in the presence of N$_2$: elucidating the role of vibrational levels. *J. Phys. Chem. C.* 2015; **119** 12815–12828.

[30] SIGLO database, www.lxcat.laplace.univ-tlse.fr; retrieved 5 May 2015.

[31] IST-Lisbon database, www.lxcat.laplace.univ-tlse.fr; retrieved 5 May 2015.

[32] Boffard JB, Jung RO, Lin CC, Wendt AE. Optical emission measurements of electron energy distributions in low-pressure argon inductively coupled plasmas. *Plasma Sources Sci. Technol.* 2010; **19**:065001.

[33] Amorim J, Baravian G, Jolly. J. Laser-induced resonance fluorescence as a diagnostic technique in non-thermal equilibrium plasmas. *J. Phys. D: Appl. Phys.* 2000; **33**:R51–R65.

[34] Es-sebbar Et, Benilan Y, Jolly A, Gazeau M-C. Characterization of an N$_2$ flowing microwave post-discharge by OES spectroscopy and determination of absolute ground-state nitrogen atom densities by TALIF. *J. Phys. D: Appl. Phys.* 2009; **42**:135206.

[35] Grob RL, Barry EF. Modern Practice of Gas Chromatography. John Wiley & Sons Inc., Hoboken, New Jersey; 2004. 1064p.

[36] Chen G, Silva T, Georgieva V, Godfroid T, Britun N, Snyders R, Delplancke-Ogletree MP. Simultaneous dissociation of CO_2 and H_2O to syngas in a surface-wave microwave discharge. *Int. J. Hydrogen Energ.* 2015; **40**:3789–3796.

[37] Pinhao NR, Janeco A, Branco JB. Influence of helium on the conversion of methane and carbon dioxide in a dielectric barrier discharge. *Plasma Chem. Plasma P.* 2014; **31**:427–439.

[38] Otake K, Kinoshita H, Kikuchi T, Suzuki R. CO_2 decomposition using electrochemical process in molten salts. *J. Phys.: Conf. Ser.* 2012; **379**:012038.

[39] Timmermans EAH, Jonkers J, Rodero A, Quintero MC, Sola A, Gamero A, Schram DC and van der Mullen J. The behavior of molecules in microwave-induced plasmas studied by optical emission spectroscopy. 2: Plasmas at reduced pressure. *Spectrochim. Acta Part B.* 1999; **54**:1085–1098.

[40] Rond C, Bultel A, Boubert P, Cheron BG. Spectroscopic measurements of nonequilibrium CO_2 plasma in RF torch. *Chem. Phys.* 2008; **354**:16–26.

[41] Silva T, Britun N, Godfroid T, Snyders R. Simple method for gas temperature determination in CO_2-containing discharges. *Opt. Lett.* 2014; **39**:6146–6149.

[42] Munoz J, Dimitrijevic MS, Yubero C, Calzada MD. Using the van der Waals broadening of spectral atomic lines to measure the gas temperature of an argon-helium microwave plasma at atmospheric pressure. *Spectrochim. Acta, Part B: At. Spectrosc.* 2009; **64**:167–172.

[43] Palomares JM, Hubner S, Carbone EAD, de Vries N, van Veldhuizen EM, Sola A, Gamero A, van der Mullen JJAM. H_β Stark broadening in cold plasmas with low electron densities calibrated with Thomson scattering. *Spectrochim. Acta, Part B: At. Spectrosc.* 2012; **73**:39–47.

[44] Konjevic N. Plasma broadening and shifting of non-hydrogenic spectral lines: present status and applications. *Phys. Rep.* 1999; **316**:339–401.

[45] Kotstka S, Roy S, Lakusta P, Mayer T, Renfro M, Gord J, Branam R. Comparison of line-peak and line-scanning excitation in two-color laser-induced-fluorescence thermometry of OH. *Appl. Opt.* 2009; **48**:6332–6343.

[46] Britun N, Godfroid T, Snyders R. Time-resolved study of pulsed Ar-N_2 and Ar-N_2-H_2 microwave surfaguide discharges using optical emission spectroscopy. *Plasma Sources Sci.Technol.* 2012; **21**:035007.

[47] Kutasi K, Guerra V, Paulo S. Theoretical insight into Ar-O_2 surface-wave microwave discharges. *J. Phys. D: Appl. Phys.* 2010; **43**:175201.

[48] Kitajima T, Nakano T, Makabe T. Increased O (^1D) metastable density in highly Ar-diluted oxygen plasmas. *Appl. Phys. Lett.* 2006; **88**:091501.

[49] Silva T, Britun N, Godfroid T, van der Mullen J, Snyders R. Study of Ar and Ar-CO$_2$ microwave surfaguide discharges by optical spectroscopy. Submitted to *J. Appl. Phys.* 2015.

[50] Rousseau A, Granier A, Gousset G, Leprince P. Microwave discharge in H$_2$: influence of H-atom density on the power balance. *J. Phys. D: Appl. Phys.* 1994; **27**:1412–1422.

[51] Subramonium P, Kushner MJ. Two-dimensional modeling of long-term transients in inductively coupled plasmas using moderate computational parallelism. I. Ar pulsed plasmas. *J. Vac. Sci. Technol. A.* 2001; **20(2)**:313–324.

[52] Bogaerts A, Kozak T, Van Laer K, Shoceckx R. FDCDU15 – carbon dioxide utilisation: plasma-based conversion of CO$_2$: current status and future challenges. *Faraday Discuss.* 2015; DOI: 10.1039/C5FD00053J.